



Mechanical analysis of a vertical-wall, semicircular-arch roadway and a repair technique using double-shell support

Tu Hong-sheng^{1,2} · Tu Shi-hao^{1,2} · Wang Chen^{1,2} · Hao Ding-yi^{1,2} · Zhu De-fu^{1,2}

Received: 18 December 2017 / Accepted: 26 June 2018 / Published online: 4 July 2018
© Springer-Verlag GmbH Germany, part of Springer Nature 2018

Abstract

Roadways in coal mines normally have two vertical side walls and a semicircular arch-shaped roof when viewed in cross section, a design conducive to the stability of surrounding rocks. The North 1 main roadway in Duerping Coal Mine has suffered severe damage and the conventional support method employed there is incapable of ensuring long-term stability of the surrounding rocks. This study provides a mechanical analysis of this vertical-wall, semicircular-arch (VWSA) roadway using a mechanical model. Formulas describing stresses in the rocks surrounding a VWSA roadway were derived through complex analysis. The stress distribution in the surrounding rocks was then predicted using the formulas. Based on the results, a double-shell support structure consisting of an internal shell, a flexible interlayer, and an external shell was developed as a new technique to stabilize surrounding rocks. The functional mechanisms of the three parts and the specific construction procedure are detailed in this paper. Moreover, the key technical parameters were optimized through a comparative analysis of the surrounding rock's deformation behavior for different shell and interlayer thicknesses. After implementation of this technique, the floor heave, relative displacement between two sides, and roof lowering in the North 1 main roadway decreased to 82, 185, and 161 mm, respectively, which meet the requirements for long-term service. This verifies the effectiveness of the proposed technique in surrounding rock control.

Keywords Vertical-wall semicircular-arch roadway · The theory of elasticity · Numerical modeling · Double-shell support · Flexible interlayer

Introduction

In China, thousands of kilometers of roadways are driven in coal mines every year (He and Qu 2016) for transport and ventilation during underground mining. Roadways with long service life, such as main roadways and drifts, are usually dug through strata with stable floor so that they can assume a stable arch cross section (Sears et al. 2017; Pengfei et al. 2016). Deformation and failure of a main roadway can disrupt the production throughout a mine. The complexity and heterogeneity of subsurface lithology, presence of geological

structures, and mining operations in adjacent coal seams have caused serious deformation of main roadways in many coal mines (Kim et al. 2018; Bloor 2013; Guo et al. 2017). Deformed roadways require frequent maintenance to be able to serve coal mines. Therefore, research is needed to provide solutions to this problem.

There are plenty of studies on the stability of rocks surrounding arched roadways. For example, He and Qu (2016) analyzed the stress and deformation characteristics of a VWSA roadway for different coefficients of lateral pressure by numerical modeling. The results showed that the compressive stress in the surrounding rocks tended to increase with increasing coefficient of lateral pressure and reached its maximum at the junctions between the vertical walls and the floor. Shuancheng et al. (2014) modeled the roof above an arched roadway as a cantilever beam and analyzed the stress states of different roof strata. The study revealed the pattern of load transfer between roof strata and suggested that the rocks at the spandrels over the roadway were most prone to deformation and failure. Shan et al. (2014) investigated the

✉ Tu Shi-hao
tsh@cumt.edu.cn

¹ State Key Laboratory of Coal Resources and Safe Mining, China University of Mining and Technology, Xuzhou 221116, Jiangsu, China

² Key Laboratory of Deep Coal Resource Mining, Ministry of Education, China University of Mining and Technology, Xuzhou 221116, Jiangsu, China

deformation and failure of the rock surrounding a VWSA roadway with a large cross section, and determined the distributions of stress and plastic zones in the surrounding rocks. Based on the results, proper parameters of rock bolt support were proposed as a solution to the problem of serious roadway deformation and the difficulty of supporting surrounding rocks. Feng et al. (2012) studied the stress state and deformation of a semicircular-arched roadway using numerical simulation software called ABAQUS. The study found that the coefficient of circumferential stress concentration is a major factor affecting the stability of the semicircular-arched roadway; as the coefficient increased, the zone of vertical stress concentration in the side walls moved towards the roof and floor, and the plastic zones in the roof and floor strata gradually increased in vertical extent. As a result, the roadway stability declined. Based on the theory of functions of a complex variable, Muskhelishvili (2013) proposed a theoretical method for estimating the stress around a hole and illustrated the distributions of stress and strain around a hole in an elastic material under different boundary conditions. Bjorkman and Richards (Bjorkman and Richards 1976, 1979; Richards and Bjorkman 1980) studied the stress field around a hole in an elastic material and the first invariant of the stress tensor when the hole was subjected to an evenly distributed load and an unevenly distributed load, separately. They also provided optimum shapes for roadway holes. Cristescu and Paraschiv (1995) investigated the patterns of stress and strain distributions in the elastic rock surrounding a cavern with a rectangular cross section and discussed the stability of surrounding rocks after the corners of the cavern's cross section were rounded off. The effects of stress and support parameters on cavern stability were analyzed for three different height-to-width ratios.

No research has looked at the mechanical behavior of VWSA roadways or provided any surrounding rock control technique using double-shell support applicable to such roadways. The North 1 main roadway in the Duerping coal mine has been heavily deformed and conventional support methods are incapable of ensuring its long-term stability. For this reason, this study proposed a double-shell support structure as new repair technique based on analysis of stress distribution in the rock surrounding this VWSA roadway and determined key technical parameters through numerical modeling. Later, this technique was applied to this main roadway and produced relatively good results.

Mechanical analysis of a VWSA roadway

Mechanical model

Since a roadway's cross-sectional dimensions are very small compared to its length, the stress analysis of a roadway can

be reduced to a planar strain problem. Moreover, because the cross-sectional area of a roadway is much smaller than the size of the space where it is, mechanical problems of a roadway can be simplified to problems of a hole in an infinite plane (Lv and Zhang 2007; Chen 1994). In the classical theory of elasticity, such problems can be analyzed using separation of variables, numerical methods for integral equations, integral transform, calculus of variations, and complex analysis (Koyama 2003). Among these methods, complex analysis has incomparable superiority when used to find analytical solutions to problems of a hole in an infinite plane (Zang et al. 2012). Figure 1 illustrates the stresses in the rock surrounding a VWSA roadway, with N_1 and N_2 indicating the directions of stresses parallel to the x -axis and the y -axis, respectively.

The body force experienced by a rock mass can be treated as a constant in the stress and displacement analysis of surrounding rocks. Therefore, the planar strain problem can be converted to the problem of solving the biharmonic equation which the stress function U has to satisfy under given boundary conditions.

$$\frac{\partial^4 U}{\partial x^4} + 2 \frac{\partial^4 U}{\partial x^2 \partial y^2} + \frac{\partial^4 U}{\partial y^4} = 0 \quad (1)$$

Let $\theta_1(z)$ and $\varphi_1(z)$ be two functions of an arbitrary complex number (complex plane) z . Goursat (1898) proposed in 1898 a complex function as the general solution to Eq. (1):

$$U = \text{Re} [\theta_1(z) + \bar{z}\varphi_1(z)] \quad (2)$$

Let the analytic function $\psi_1(z) = \theta_1'(z)$, then the stress components can be written as:

$$\begin{cases} \sigma_x + \sigma_y = 4 \text{Re} [\varphi_1'(z)] \\ \sigma_y - \sigma_x + 2i\tau_{xy} = 2[\bar{z}\varphi_1''(z) + \psi_1'(z)] \end{cases} \quad (3)$$

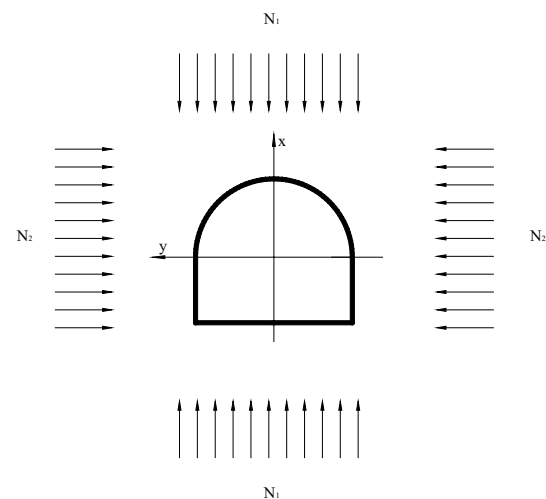


Fig. 1 Schematic of stresses in the rock surrounding a VWSA roadway

Imposing the rules for operations of complex numbers and solving Eq. (3) yield the stress components:

$$\begin{cases} \sigma_x = 2 \operatorname{Re} [\varphi_1'(z)] - \operatorname{Re} [\bar{z}\varphi_1''(z) + \psi_1'(z)] \\ \sigma_y = 2 \operatorname{Re} [\varphi_1'(z)] + \operatorname{Re} [\bar{z}\varphi_1''(z) + \psi_1'(z)] \\ \tau_{xy} = \operatorname{Im} [\bar{z}\varphi_1''(z) + \psi_1'(z)] \end{cases} \quad (4)$$

and displacement components:

$$\frac{E}{1 + \mu}(u + iv) = (3 - 4\mu)\varphi_1(z) - \overline{z\varphi_1'(z)} - \overline{\psi_1(z)} \quad (5)$$

The stress and displacement should satisfy the following boundary conditions:

$$\varphi_1(t) + \overline{t\varphi_1'(t)} + \overline{\psi_1(t)} = i \int_A^B (X + iY)ds \quad (6)$$

$$\frac{E}{1 + \mu}(\bar{u} + i\bar{v}) = (3 - 4\mu)\varphi_1(t) - \overline{z\varphi_1'(t)} - \overline{\psi_1(t)}, \quad (7)$$

where E is elastic modulus; μ is Poisson’s ratio; t is a boundary value; A denotes the initial point for integration on the boundary; B is an arbitrary point on the boundary except A ; X is the component of the surface force acting over the boundary in the x -direction; and Y is the component of the surface force in the y -direction.

In an infinite domain with a single hole, if the stress at a point infinitely distant from the hole boundary is bounded, then we have:

$$\begin{cases} \varphi_1(z) = -\frac{1}{8\pi(1 - \mu)}(X + iY) \ln z + \left(\frac{N_1 + N_2}{4}\right)z + \varphi_1^0(z) \\ \psi_1(z) = \frac{1}{8\pi(1 - \mu)}(X - iY) \ln z + \left(-\frac{(N_1 - N_2)e^{-2i\beta}}{2}\right)z + \psi_1^0(z) \end{cases}, \quad (8)$$

where β is the angle between the principal stress N_1 and the x -axis, $\varphi_1^0(z) = \sum_{n=0}^{\infty} \frac{a_n}{z^n}$ and $\psi_1^0(z) = \sum_{n=0}^{\infty} \frac{b_n}{z^n}$ are two single-valued analytic functions at infinity.

Solution of the mechanical model

The application of complex analysis to solving the aforementioned mechanical problem involves transforming the cross section of the VWSA roadway to a circular one through conformal mapping. To this end, a conformal map $z = \omega(\zeta)$ is employed to transform the complex shape boundary of the roadway in the complex plane z into a unit circle in the complex plane ζ (Fig. 2).

Let the function $\varphi(\zeta) = \varphi_1(z)$, $\psi(\zeta) = \psi_1(z)$, and by the function transformation of complex plane z with complex plane ζ , then we have:

$$\begin{cases} \varphi(\zeta) = \varphi_1(z) = \varphi_1[\omega(\zeta)] \\ \psi(\zeta) = \psi_1(z) = \psi_1[\omega(\zeta)] \end{cases} \quad (9)$$

Let the function $\Phi(\zeta) = \varphi_1'(z)$, $\Psi(\zeta) = \psi_1'(z)$, and then we have:

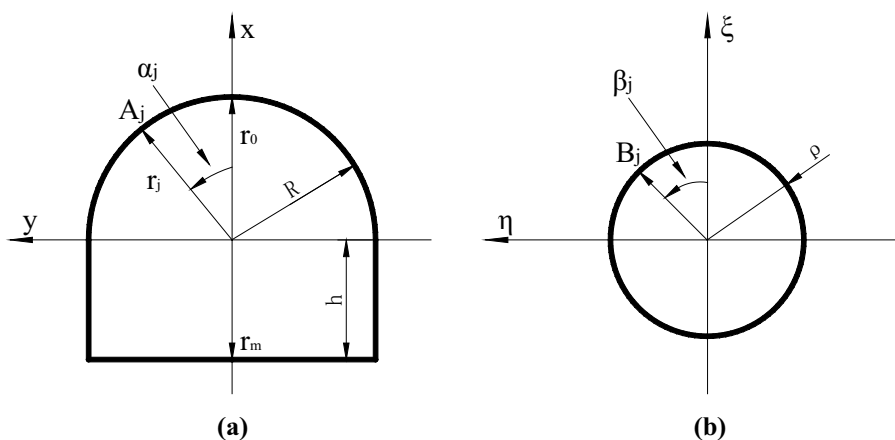
$$\begin{cases} \Phi(\zeta) = \varphi_1'(z) = \frac{\varphi'(\zeta)}{\omega'(\zeta)} \\ \Psi(\zeta) = \psi_1'(z) = \frac{\psi'(\zeta)}{\omega'(\zeta)} \end{cases} \quad (10)$$

So, the Eq. (3) can be rewritten as:

$$\begin{cases} \sigma_\xi + \sigma_\eta = 4 \operatorname{Re} [\Phi(\zeta)] \\ \sigma_\eta - \sigma_\xi + 2i\tau_{\xi\eta} = \frac{2}{\omega'(\zeta)} [\overline{\omega'(\zeta)}\Phi'(\zeta) + \omega'(\zeta)\Psi(\zeta)] \end{cases} \quad (11)$$

In Fig. 2, R is the radius of the semicircular arch of the roadway, h is the height of the vertical walls, and ρ is the radius of the unit circle. Let (r_j, α_j) be the polar coordinates

Fig. 2 Transformation of a VWSA roadway onto a unit circle in the complex plane



of the j th point on the boundary of the roadway, denoted A_j , and $(1, \beta_j)$ be the polar coordinates of the point on the unit circle that corresponds to it, B_j . The polar coordinates of the first point on the roadway's boundary in the complex plane z, A_0 , and the corresponding point on the complex plane ζ, B_0 , are $(r_0, 0)$ and $(1, 0)$, respectively. Assume that $g(\zeta)$ is an analytic function within the unit circle and then integrate it anticlockwise. Then the conformal map (ξ and η axes) is expanded into a Laurent series:

$$\begin{cases} \psi(\zeta) = -\bar{\omega}\left(\frac{1}{\zeta}\right)\varphi_0'(\zeta)/\omega'(\zeta) + 1.5105\zeta - 0.0041\zeta^2 - 0.0114\zeta^3 - 25.09\zeta^{-1} - 0.028 \\ \varphi(\zeta) = 12.544\zeta + 0.5103\zeta^{-1} - 0.7805\zeta^{-2} + 0.8769\zeta^{-3} - 0.3763\zeta^{-4} - 0.1255\zeta^{-5} - 0.251 \end{cases} \quad (13)$$

$$z = \omega(\zeta) = 2.23(\zeta - 0.02 - 0.05\zeta^{-1} + 0.06\zeta^{-2} - 0.069\zeta^{-3} + 0.03\zeta^{-4} + 0.01\zeta^{-5}) \quad (12)$$

An arbitrary point in z can be expressed as $(x + iy)$. An arbitrary point in ζ can be written as $(\xi + i\eta)$, with $\xi^2 + \eta^2 = 1$. Then cross section of the VWSA roadway is transformed by substituting $z = x + iy$ and $\zeta = \xi + i\eta$ into Eqs. (9) and (10) and then separating the real and imaginary parts. The shape of the roadway's cross section after transformation is shown in Fig. 3.

Increasing the number of terms of the series can reduce the difference in shape between the roadway's cross sections before and after the conformal transformation, but it

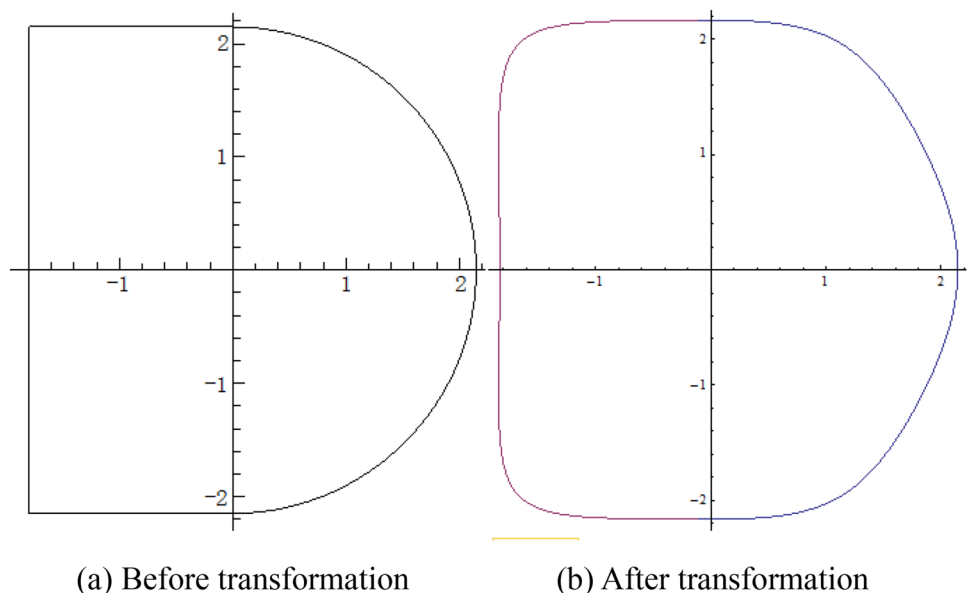
also increases the complexity of the problem solving process several fold. Figure 3 compares the cross sections of the roadway before and after the conformal transformation of the first six terms of the series. It is clear that the shape of the cross section after transformation is similar to that before transformation and the degree of similarity between is sufficient for solving mining engineering problems. After that, the expressions for the stress functions are obtained by further solving Eqs. (1)–(9). The stress functions have the following forms:

Substituted Eqs. (12) and (13) into Eqs. (9)–(11) and then stress components have the following forms:

$$\begin{cases} \sigma_\xi = \text{Re} \left\{ \frac{2}{\omega'(\zeta)} \left[\overline{\omega'(\zeta)}\Phi'(\zeta) + \omega'(\zeta)\Psi(\zeta) \right] - 4 \text{Re} [\Phi(\zeta)] \right\} \\ \sigma_\eta = \text{Re} \left\{ \frac{2}{\omega'(\zeta)} \left[\overline{\omega'(\zeta)}\Phi'(\zeta) + \omega'(\zeta)\Psi(\zeta) \right] + 4 \text{Re} [\Phi(\zeta)] \right\} \\ \tau_{\xi\eta} = \text{Im} \left\{ \frac{1}{\omega'(\zeta)} \left[\overline{\omega'(\zeta)}\Phi'(\zeta) + \omega'(\zeta)\Psi(\zeta) \right] \right\} \end{cases} \quad (14)$$

Values of the parameters included in Eq. (14) are as follows: burial depth of the roadway 400 m; bulk density of overlying strata 2500 kg/m^3 ; coefficient of lateral pressure

Fig. 3 Cross sections of the roadway before and after the conformal transformation



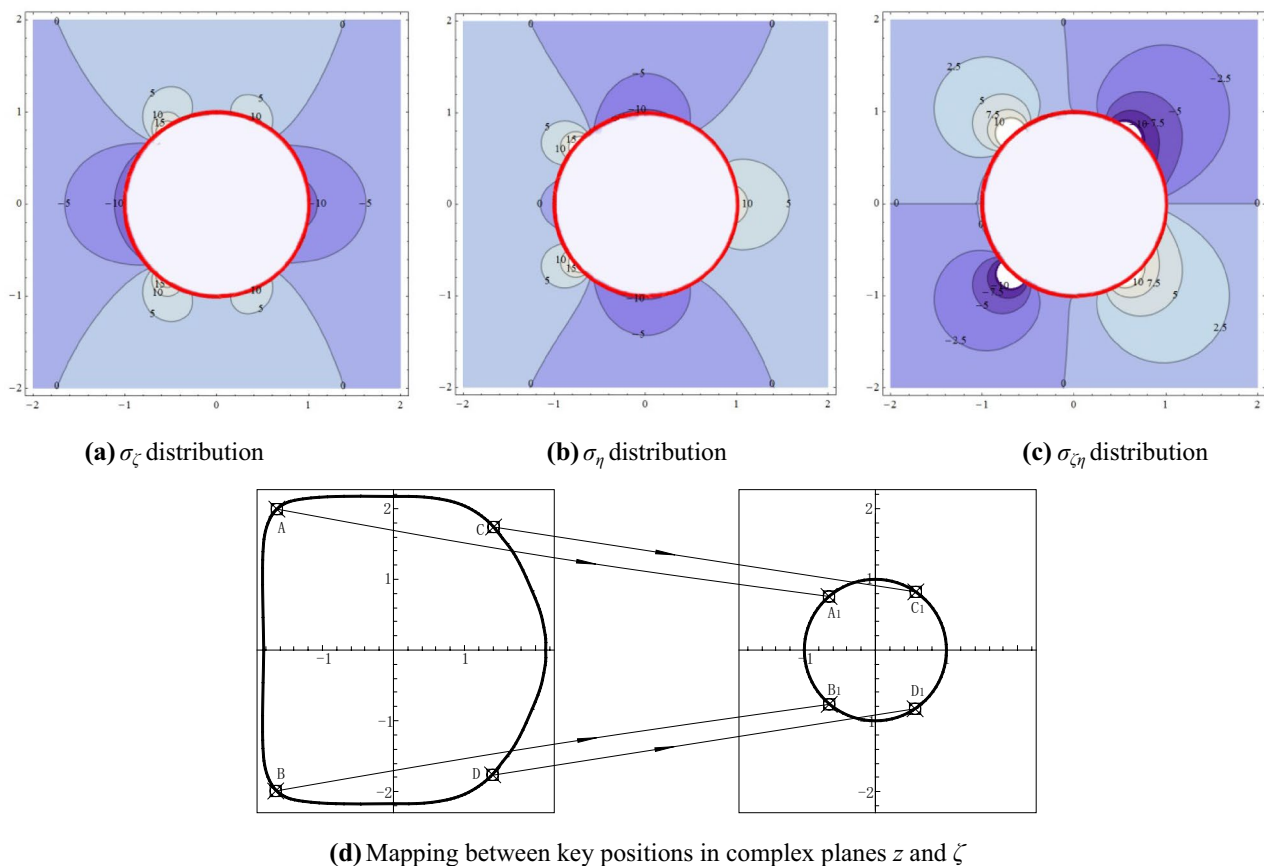


Fig. 4 Contours of stress around the roadway

0.8; elastic modulus 12.1 GPa; Poisson’s ratio 0.3; radius of the semicircular arch 2.15 m; and wall height 1.85 m. Combining with the corresponding relation of stress components in the Eq. (4), the stress distribution around the roadway was then estimated and plotted as stress contours in Fig. 4.

As seen in Fig. 4, stress is concentrated to varying degrees in the rock surrounding the VWSA roadway. Vertical stress is concentrated primarily at the four corners indicated by A, B, C, and D in Fig. 4d, with a maximum stress concentration factor of 1.5. Horizontal stress concentration occurs at corners A and B as well as in the two side walls and the roof, with a maximum stress concentration factor of about 1.88. Shear stress concentration is also found at corners A, B, C, and D.

Project overview

Conditions of the main roadway

In Duerping Coal Mine of Xishan Coal Electricity Group, the North 1 main roadway serves working faces in coal seam 3#. This roadway was driven through the relatively stable

limestone strata underlying coal seam 3# (Fig. 5) and the originally reinforce only by 250-mm-thick masonry-lining supporting. However, the joints of surrounding rocks in the zone located 3800–4900 m from the head of this main roadway were well developed in the influence of high in situ stress due to fault, fold and the mining of the adjacent seam. And the main roadway has been seriously deformed and fractured. Having been repaired for many times, this main roadway can barely function normally and is expected to serve for the ensuing 20–25 years. It is 380–420 m deep underground, averaging 400 m, and has a design width and height of 4.3 and 4.0 m, respectively.

Deformation characteristics of the main roadway

Field measurements showed that the roof had been fractured and sunken substantially. The maximum roof lowering reached about 1/6 of the design height of the roadway, and the maximum floor heave was 300 mm. Moreover, the minimum distance between the two sides was 3600 mm, representing a relative lateral displacement of 700 mm. The zone of serious deformation was repaired using the conventional support method. Anchor bolts and roof lowering cables with

Fig. 5 Stratigraphic column

No.	Stratigraphic column	Rock type	Thickness(m)	Lithological characteristics
1		Mudstone	5	Ash black, joint development
2		Siltstone	2	Brownish red, lower part contains silt
3		Mudstone	10	Black gray, joint development
4		Coal 3#	1.3	Black, simple structure
5		Mudstone	3	Black gray, joint development
6		Limestone	13.5	Dark grey, clumpy structure
7		Mudstone	1	Black gray, joint development
8		Limestone	10	Dark grey, clumpy structure
9		Siltstone	5	Brownish red, lower part contains silt

wire mesh were installed to stabilize the two sides and the roof. The original support parameter's details for repaired roadway are as follows: the diameter and the length of the deformed steel bar bolt are 20 and 1800 mm, respectively, the inter-row spacing of the bolt is 1000 mm × 1000 mm. The diameter and the length of the deformed wire rope anchor cables are 17.8 and 5300 mm, respectively, the row spacing of the cable is 1000 mm, and the cables, respectively, be installed in the center of roof and two sides. However, due to the dynamic pressure arising from mining, the main roadway still underwent an increasing amount of deformation and was deemed to be unable to maintain stability in the long term. After using this traditional reinforcing method, a large number of the rock bolts and cables failed because the surrounding rocks were still subjected to great forces. Figure 6

shows the deformation characteristics of the roadway and the supports installed for repair.

Principle of the double-shell support structure

Definition of double-shell support

To deal with the problems in the conventional repair method, a new support method using a double-shell support structure was proposed. In this method, concrete is applied to the surrounding rocks by grouting and spraying to form two closed reinforcing shells, an internal shell and an external one. A flexible interlayer composed primarily of fractured

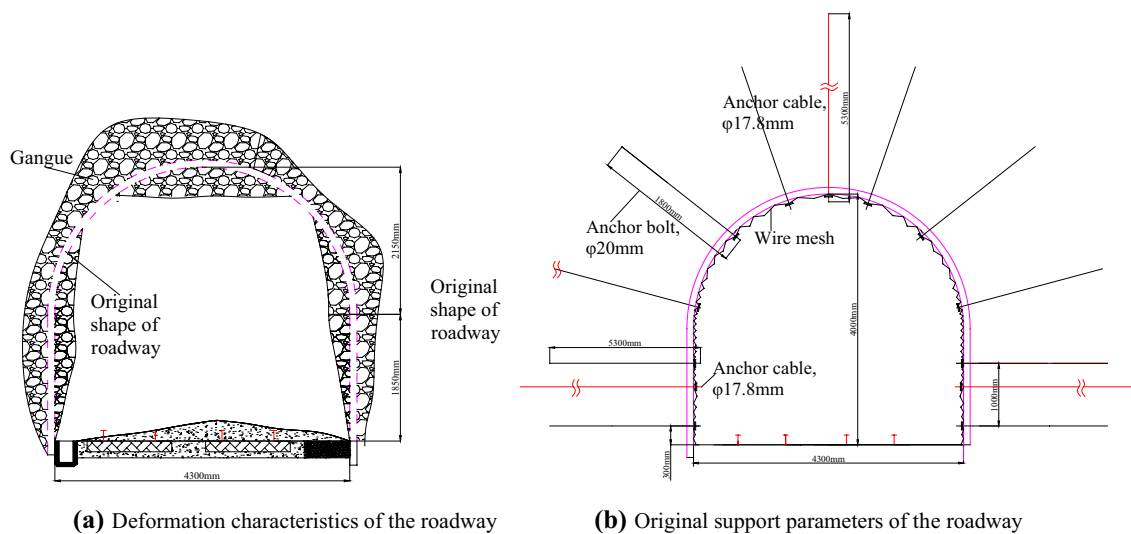


Fig. 6 Deformation characteristics and the original support parameters of the roadway

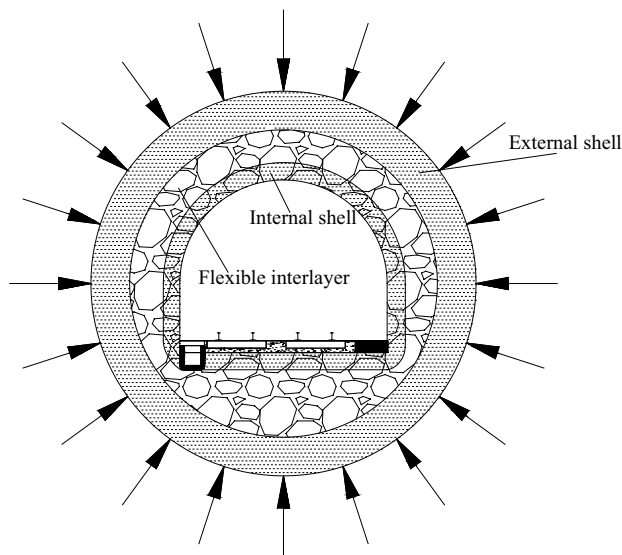


Fig. 7 The schematic of double-shell support method

rock masses can be created between the two shells by adjusting the technical parameters used in grouting. The two shells with high compressive strengths and the flexible interlayer then constitute a yieldable structure that can withstand large deformation. This structure is then combined with anchor bolts and cables as a supplement. The schematic of this method is shown in Fig. 7.

Construction procedure

Given that the broken rock masses supported only by rock bolts and cables can not restore structural integrity and thus have low bearing capacity, it is necessary to provide stronger primary supports to the surrounding rocks over the complete cross section of the roadway, to structurally reinforce the surrounding rocks. The purpose of grouting involved in the proposed method is to combine the interior broken rock masses into a complete block and thereby increase the bearing capacity of the surrounding rocks. The resulting internal shell not only enables the interior of surrounding rocks to support greater rock pressure, but also acts as a firm foundation for the rock bolts. The external shell covering the roadway surface is intended to prevent the rock exposed at the roadway surface coming into direct contact with the air, thus slowing down the weathering of the surface rock and protecting it from destabilizing. The flexible interlayer serves to absorb the strain energy stored by the surrounding rocks under high stress and thereby reduce damage to the surface. The specific construction procedure is described below:

1. The first step is to create the internal shell on the roadway surface so that the grout later placed into the interior regions will not flow out along the fractures in the broken surrounding rocks. Before spraying the shotcrete, a wire mesh is fixed onto the roadway surface to keep overlying broken strata from falling and thereby prevent further surface deformation.
2. The next step is to grout the external shell using grouting bolts, to bond the rock masses at the ends of the bolts to form an integrated block, called internal load-bearing shell. This shell can improve the bearing capacity of the surrounding rocks.

Determination of key technical parameters

The analysis above suggests that the effectiveness of the double-shell support structure in surrounding rock control depends on the thicknesses of the external shell, flexible interlayer, and internal shell. The purpose of the flexible interlayer is to compensate for the deformation caused by the action of high stress from the interior upon the surface of the surrounding rocks. If it is too thick, the fractured rock masses between the two shells will not be compacted after the deformation stops. In this case, the connections between the rock masses and the shells are loose, which has an adverse effect on roadway stability. If its thickness is too small, the flexible interlayer will be unable to efficiently absorb the strain energy stored by the surrounding rocks, thus leading to further damage to the surface rock. For these reasons, a numerical analysis was performed with FLAC3D to study the effects of the aforementioned three parameters on roadway stability.

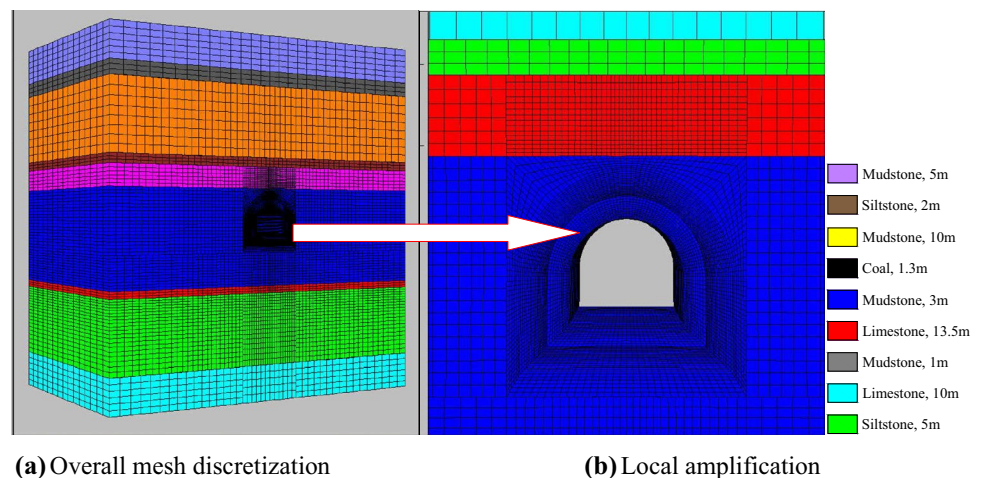
Numerical modeling

The surrounding rocks and VWSA roadway were modeled with a Mohr–Coulomb constitutive model. This model has dimensions of $55 \text{ m} \times 40 \text{ m} \times 5 \text{ m}$ (length \times width \times height). Its four sides and bottom are the displacement boundaries and the top is the stress boundary.

To conveniently changing the strata parameters of double-shell in the numerical modeling process, the surrounding rocks within 5 m of roadway be meshing in divergent shape of equally spacing, and spacing is 0.1 m. Internal shell and external shell, respectively, are created by grouting and shotcreting, and the strata parameters are different from the rock strata. The strata parameters of internal shell, flexible interlayer and external shell were determined according to laboratory experiments. The physico-mechanical parameters of different strata are provided in Table 1. The model was

Table 1 Physical and mechanical parameters of coal and rocks

Rock type	Thickness/m	Tensile strength /MPa	Bulk modulus/GPa	Shear modulus /GPa	Cohesion/MPa	Frictional angle/°	Bulk forces/kg/m ³
Mudstone	5	0.4	4.8	3.1	2.8	21	2150
Siltstone	2	1.7	8.2	5.8	4.95	32	2550
Mudstone	10	0.5	4.1	2.5	2.3	22	2300
Coal 3#	1.3	0.18	1.6	1.2	1.8	17	1390
Mudstone	3	0.3	3.9	2.3	2.7	23	2100
Limestone	13.5	1.5	7.0	5.0	4.58	28	2500
Mudstone	1	0.3	4.3	1.9	2.8	22	2000
Limestone	10	1.2	6.9	4.5	4.31	29	2450
Siltstone	5	1.7	8.5	5.2	5.35	30	2400
External shell	0.6–1.2	0.8	5.5	3.9	3.7	31	2460
Flexible interlayer	0.3–0.9	0	0.16	0.08	0.064	34	1210
Internal shell	0.1–0.7	0.59	3.8	3.2	2.9	30	2455

Fig. 8 Mesh discretization of the numerical model

discretized by a mesh into a total of 193,230 elements, as shown in Fig. 8.

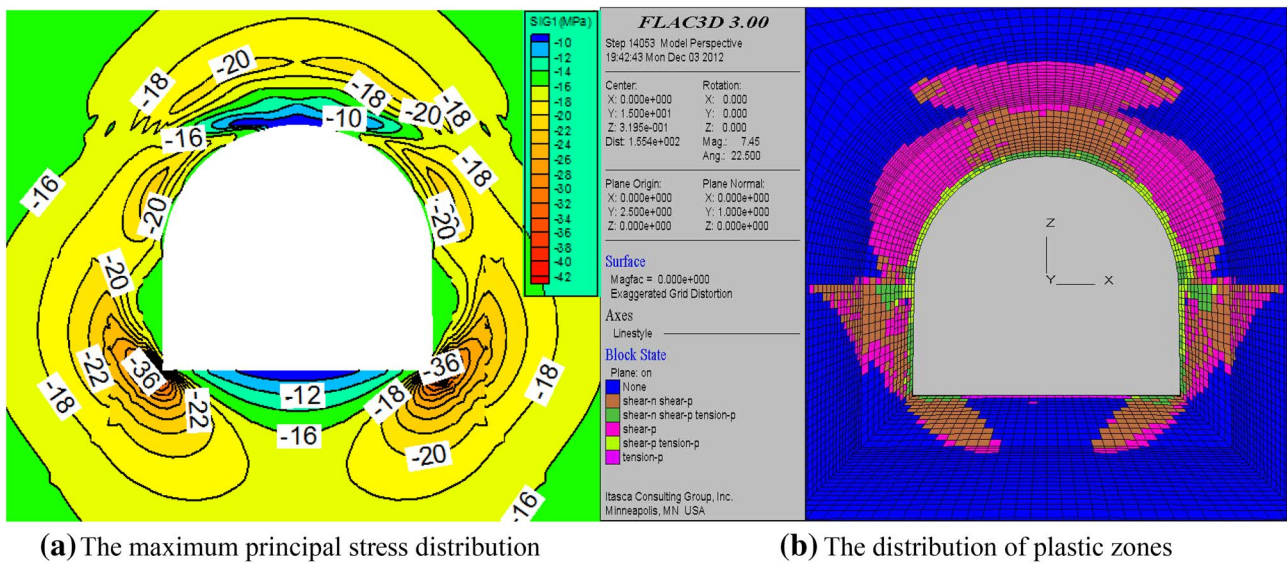
Original failure features and anchor bolt parameter's design with double-shell support

Figure 9 shows the stress distribution and distribution of plastic zones in surrounding rocks of roadway with the same supporting parameters in Fig. 6b. For convenience, to analyze and identify the figures, the anchor bolts and cables will be set invisible in the figures.

Figure 19 shows that the stress contour of maximum principal was discontinuous, and in some areas appeared the phenomenon of mutations. Obvious stress concentration area was located at the two sides of lower corners and the two spandrels over the arch. The farther the distance from the surface of roadway, the lower stress concentration degree.

The plastic zones located at the two sides of lower corners and the two spandrels over the arch were well developed, and the unstable rock strata of roadway were difficult to meet the normal use.

The primarily failure and stress concentration zones were two sides of lower corners and the two spandrels over the arch according to the mechanical analysis of VWSA roadway in part 2. So, we should reinforce the supporting parameters in these zones to improve the stress and deformation characteristics. The final anchor bolts and cables of support parameter's details for repaired VWSA are as follows: the diameter and the length of the deformed steel bar bolt are 20 and 1800 mm, respectively, the inter-row spacing of the bolt is 800 mm × 800 mm in two sides and roof, the inter-row spacing of the bolt is 1000 mm × 800 mm in floor. The diameter and the length of the deformed wire rope anchor cables are 17.8 and 5300 mm, respectively, the row spacing of the cable is 800 mm, and the cables, respectively, are

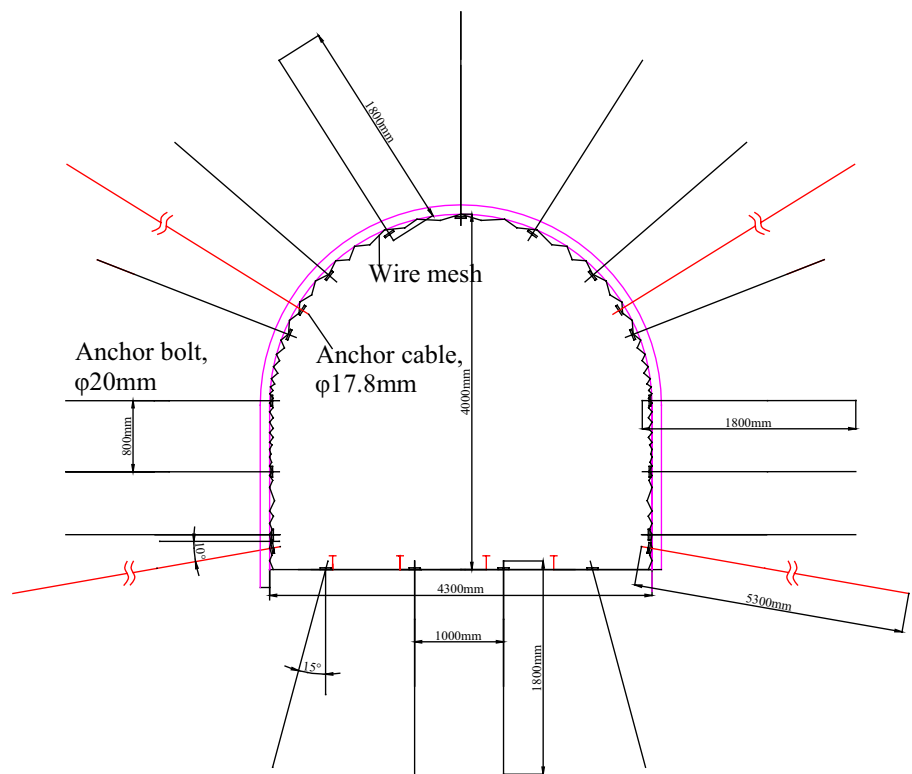


(a) The maximum principal stress distribution

(b) The distribution of plastic zones

Fig. 9 Original stress and plastic zone’s distribution with traditional reinforcing method

Fig. 10 The design of bolts and cables in double-shell support roadway



installed in the two sides of lower corners and the two span-
 drels over the arch. These support parameters of anchor bolts
 and cables will be used in the following research figures.

Figure 10 shows the detailed support parameters of the road-
 way as we designed.

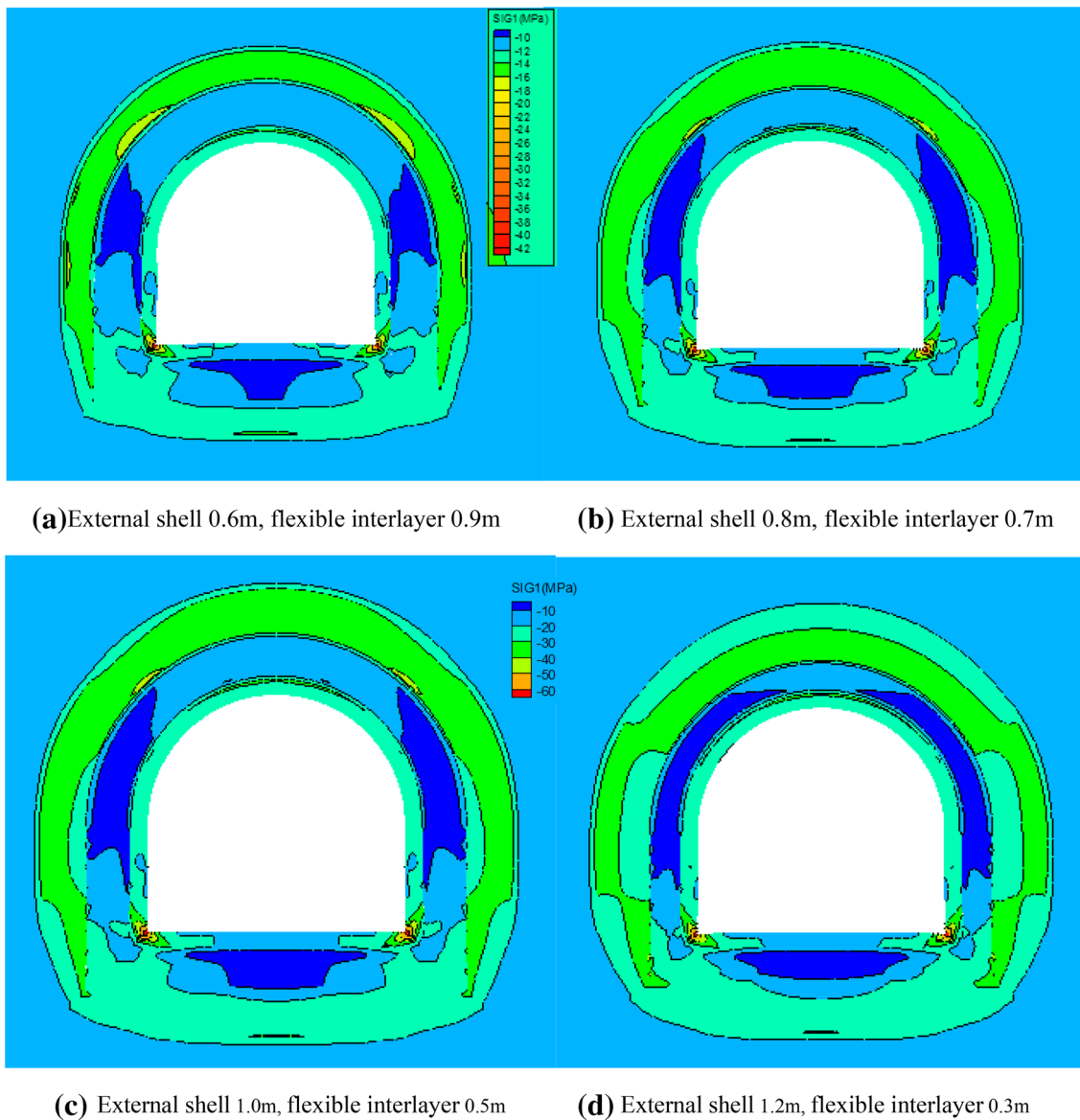


Fig. 11 The maximum principal stress distribution

Effects of thicknesses of the external shell and flexible interlayer on roadway stability

The effect of each of the three parameters was studied by controlling for other parameters. One function of the internal shell is to provide a reliable foundation for the rock bolts. First, the internal shell thickness, which normally ranges from 0.1 to 0.7 m, was held constant at 0.5 m. Then the stress and deformation characteristics of the surrounding rocks were studied by changing the thicknesses of the external shell (0.6, 0.8, 1.0, and 1.2 m) and the flexible interlayer (0.9, 0.7, 0.5, and 0.3 m).

Distribution of maximum principal stress in the surrounding rocks

Figure 11 shows that the maximum principal stress was concentrated primarily around the shells and peaked at the lower corners of the roadway. The stress intensity was much greater in the two shells than in the flexible interlayer, demonstrating high rigidity of the shells and high yield strength of the interlayer. Changes in the thicknesses of the external shell and flexible interlayer were found to affect the principal stress distribution in the internal shell slightly, but have relatively significant effects on the external shell and flexible interlayer. The thicker the external shell, the lower the principal stress in it and the smaller the stress concentration

zone. When external shell thickness was 0.6, 0.8, 1.0, and 1.2 m, the stress concentration zone accounted for 91, 56, 50, and 47%, respectively, of the volume of the whole shell. Obviously, when the external shell was thicker than 0.8 m, its thickness had only a small influence on stress distribution in the shell. When the flexible interlayer thickness was 0.9, 0.7, 0.5, and 0.3 m, the compressive zone (subjected to

a relatively large force) made up about 20, 62, 71, and 82%, respectively, of the total volume of this interlayer. It is reasonable to infer from the results that the compressive zone in the flexible interlayer will be too small to ensure roadway stability when the interlayer thickness is larger than 0.7 m, whereas it will be too large to maintain energy absorption capacity in the long term if the interlayer thickness is less

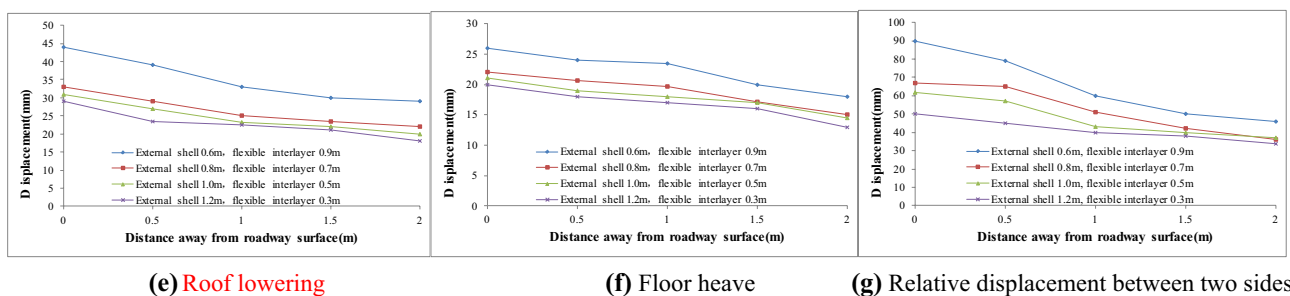
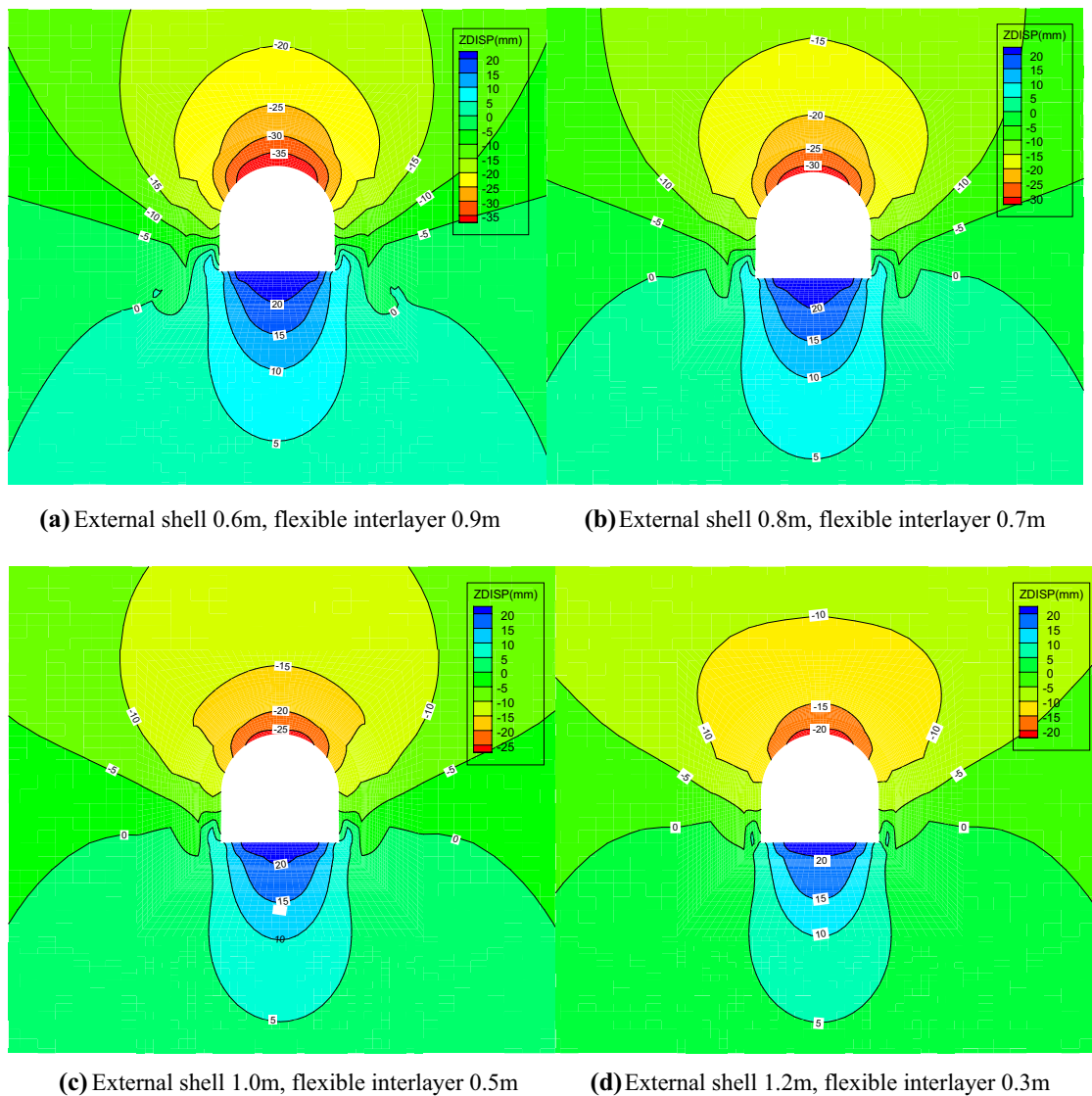


Fig. 12 Displacement distribution of different location away from the roadway’s surface

than 0.5 m. Therefore, the appropriate thickness for the flexible interlayer should be between 0.5 and 0.7 m.

Deformation characteristics of the surrounding rocks

The amount of deformation of the surrounding rocks decreased with increasing external shell thickness and also with increasing distance from the roadway surface (Fig. 12). When the external shell thickness was greater than 0.8 m, the rate of change in deformation declined sharply, indicating that an external shell thicker than 0.8 m is unable to

effectively reduce deformation. The deformation characteristics indicate that the external shell thickness has only a small effect on the deformation of the floor strata, but it significantly affects the deformation of the two vertical walls. Its effect tends to weaken with increasing distance from the roadway surface.

Distribution of plastic zones in the surrounding rocks

As seen in Fig. 13, the distribution of plastic zones in the surrounding rocks varied little with the thicknesses of the

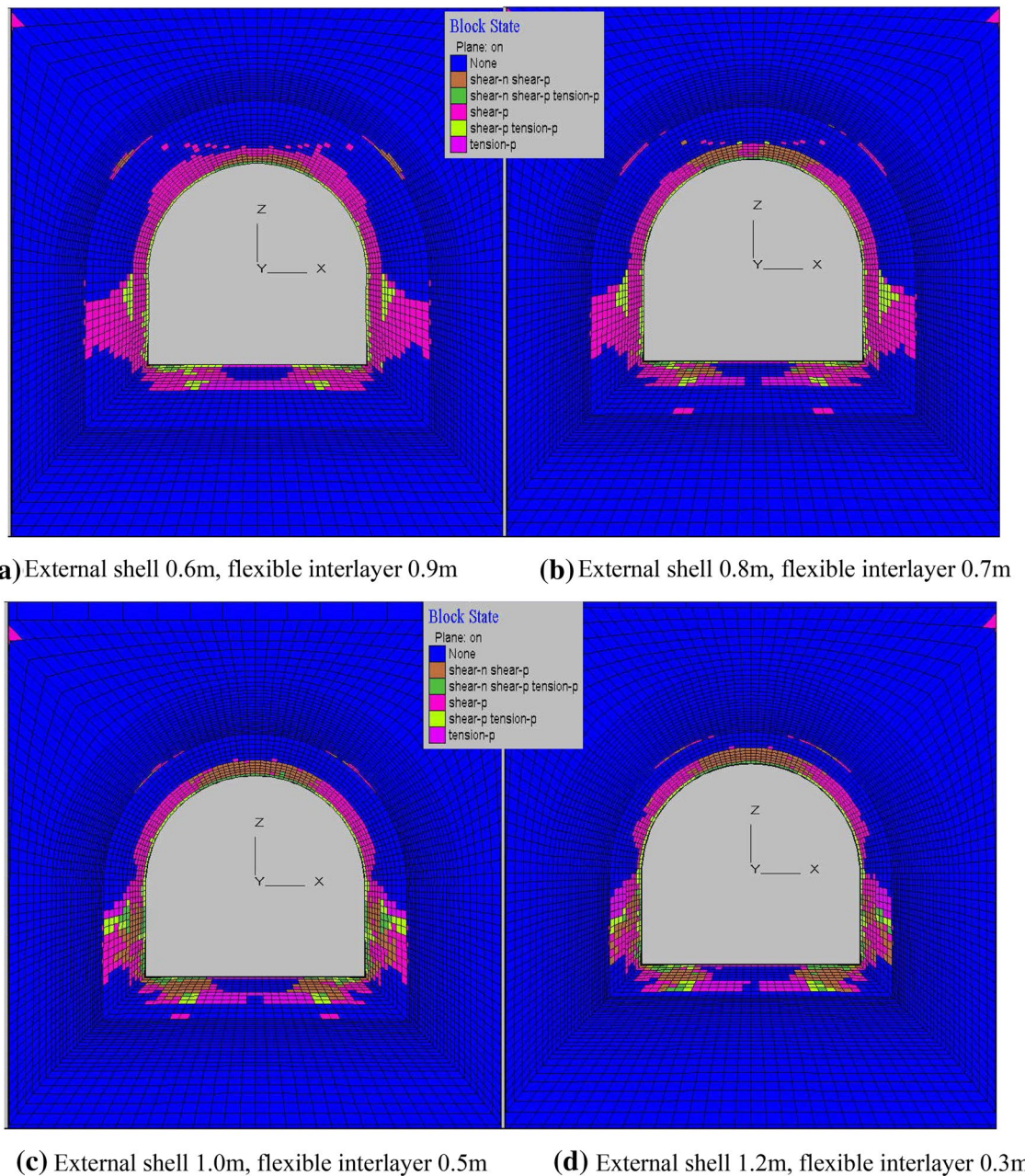


Fig. 13 The distribution of plastic zones

external shell and the flexible interlayer. There is apparent plastic deformation in the region within 0.1 m of the roadway surface, primarily in the side walls and the floor. The figure reveals different failure modes of the surrounding rocks in different locations. The internal shell failed primarily due to shear, while the flexible interlayer mainly failed in shear and tension. When the external shell was thinner than 0.8 m, the flexible interlayer along the vertical walls exhibited small-scale shear failure and tensile failure. When the external shell thickness was larger than 0.8 m, the zones of shear failure and tensile failure along the vertical walls expanded rapidly. Because the shear and tensile strengths of the surrounding rocks are smaller than

their compressive strengths, the external shell thickness should not exceed 0.8 m to achieve effective stabilization.

A smaller interlayer thickness means a larger zone to be grouted, a higher construction cost, and greater difficulty in controlling the amount of grout to be applied and grout outflow. Based on the results presented above, the optimal thicknesses for the external shell and flexible interlayer were set at 0.8 and 0.7 m, respectively.

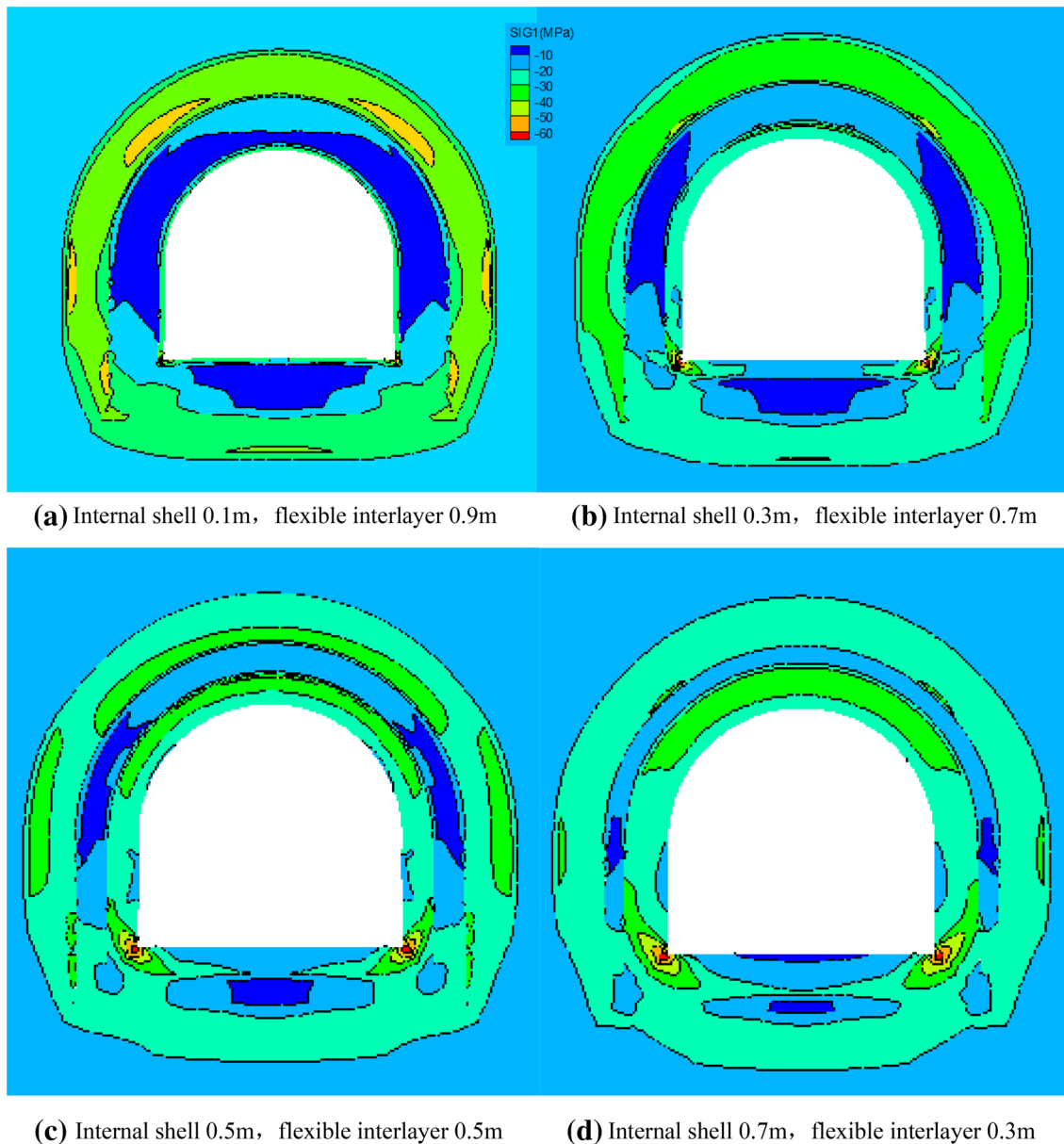


Fig. 14 The maximum principal stress distribution

Effects of thicknesses of the internal shell and flexible interlayer on roadway stability

When analyzing the effects of thickness of the internal shell and flexible interlayer, the external shell thickness stayed constant at the optimal value, i.e., 0.8 m. Then the stress and deformation characteristics of the surrounding rocks were studied for different internal shell thicknesses (0.1, 0.3, 0.5, and 0.7 m) and flexible interlayer thicknesses (0.9, 0.7, 0.5, and 0.3 m).

Distribution of maximum principal stress in the surrounding rocks

As the thicknesses of the internal shell and flexible interlayer changed, the pattern of stress distribution in the surrounding rocks varied markedly (Fig. 14). Stress concentration occurred mainly around the lower corners of the roadway. When the internal shell was 0.1–0.3 m thick, the principal stress in it varied little with its thickness. As its thickness increased from 0.5 to 0.7 m, the principal stress distribution varied relatively obviously. A larger internal shell thickness is associated with a larger stress concentration zone. When the internal shell thickness was 0.1, 0.3, 0.5, and 0.7 m, the stress concentration zone accounted for 10, 20, 58, and 89%, respectively, of the volume of the whole internal shell. Clearly, the stress concentration zone in the internal shell grew in size substantially after the shell thickness exceeded 0.3 m. When the flexible interlayer was 0.9, 0.7, 0.5, and 0.3 m thick, the stress concentration zone made up 18, 26, 82, and 93%, respectively, of the whole interlayer. As the interlayer thickness decreased from 0.7 to 0.3 m, the stress concentration zone suddenly expanded. Therefore, the optimal thicknesses for the internal shell and the flexible interlayer were set at 0.3 and 0.7 m, respectively.

Deformation characteristics of the surrounding rocks

Overall, the amount of deformation of the surrounding rocks decreased with increasing internal shell thickness and with increasing distance from the roadway surface (Fig. 15). When the internal shell thickness was greater than 0.3 m, the roadway showed a noticeable decrease in roof deformation. This implies that an internal shell thicker than 0.3 m is ineffective in controlling the deformation of the surrounding rocks. The floor deformation did not substantially decrease with increasing thickness of the internal shell. The two side walls underwent the most significant deformation (measured by relative displacement between two sides), followed by the roof strata (roof lowering). The floor heave was smaller than the roof lowering and relative displacement between two sides.

Distribution of plastic zones in the surrounding rocks

Figure 16 reveals that the distribution of plastic zones in the surrounding rocks varied significantly with the thicknesses of the internal shell and flexible interlayer. When the internal shell was 0.1 m thick, the external shell and the interlayer experienced severe failure in tension and shear, indicating a lack of stability of the surrounding rocks. When the internal shell was 0.3 m thick, the plastic zones in the surrounding rocks significantly reduced in size. They were distributed mainly in the two side walls and the floor. Localized shear failure took place in the roof. Small zones of tensile failure were found in the flexible interlayer. As the internal shell thickness increased from 0.5 to 0.7 m, the plastic zones in the side walls and along the corners further expanded. Since smaller zones of plastic deformation in the surrounding rocks are associated with higher roadway stability, 0.3 m was supposed to be a proper thickness for the internal shell.

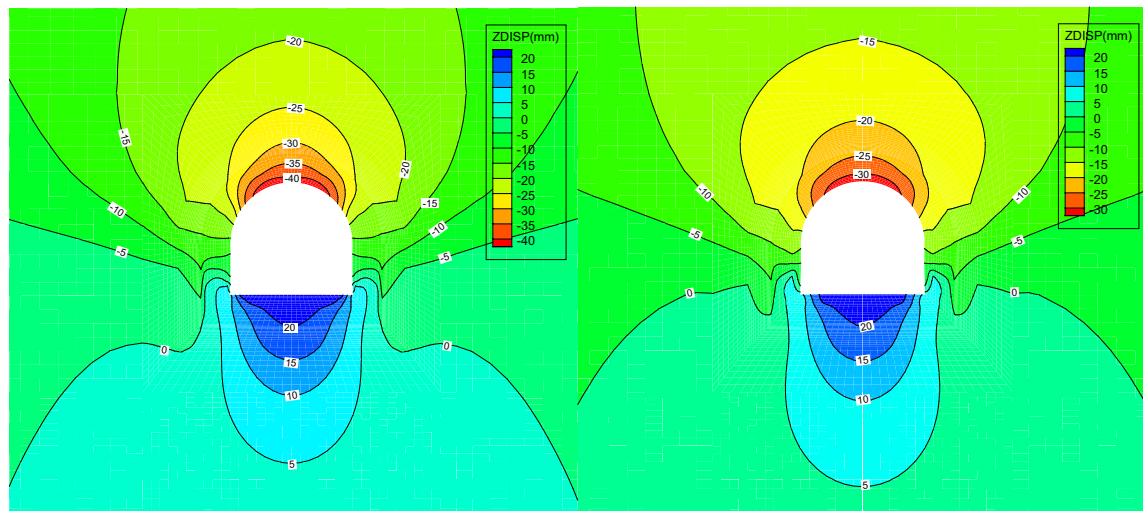
The analysis above suggests that the optimal thicknesses for the internal shell, flexible interlayer, and external shell could be 0.3, 0.7, and 0.8 m, respectively.

Effectiveness of the double-shell support

To verify the validity of the optimal thicknesses determined, the double-shell support technique was applied to the North 1 main roadway. The grout and shotcrete for the internal and external shells were prepared by mixing 525# ordinary Portland cement with 40 Be sodium silicate in a mass ratio of 1:0.03–1:0.05. The shotcrete was sprayed with a Hsp-5 shotcrete machine, a blast-proof shotcrete machine for wet spraying. The grout was placed using grouting bolts combined with KBY-50/70 hydraulic grouting pumps. The grouting bolts are hollow anchor bolts whose outer wall is used for stabilization and hole sealing and inner shaft serves to deliver grout. The grouting bolts, made of seamless tubes, have a diameter of 22 mm, wall thickness of 3 mm, and length of 1.8 m (Fig. 17).

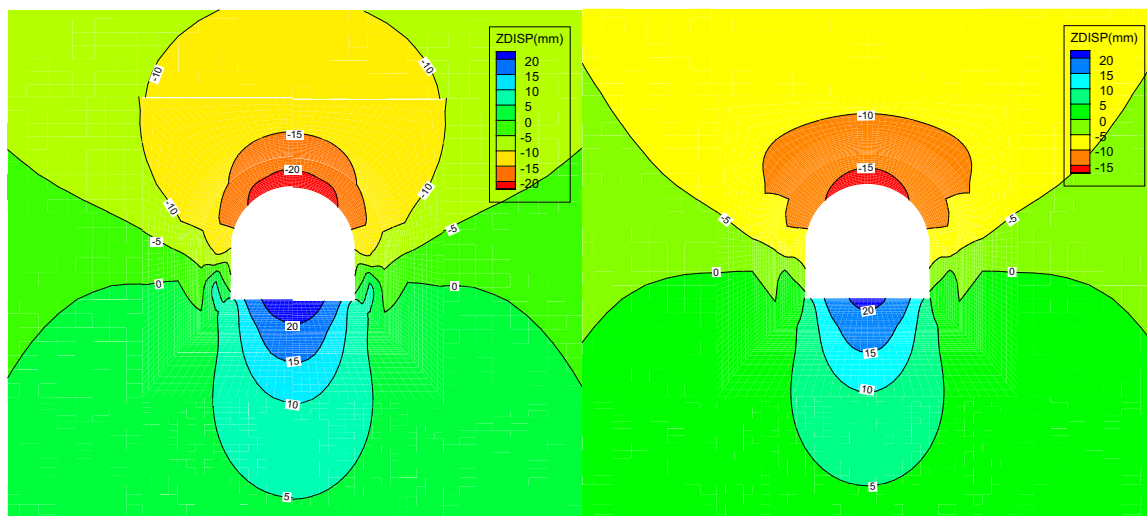
The supporting processes of roadway were: hanging wire mesh (100 mm × 100 mm, 5 mm in diameter) on the surface of roadway, installed grouting bolts, grouting internal shell with the thickness of 30 cm, grouting and forming the external shell and installed anchor cables.

The technique was experimentally implemented throughout a 20-m long segment of the main roadway. Three equally spaced cross sections were selected along this segment as observation stations. Then the displacements of the roadway surface and separations between layers in the roof were measured once a day at the observation stations during the period between January 20, 2016 and March 31, 2016. The averages of displacements observed at the three stations are plotted in Fig. 16, where the deep base point displacements



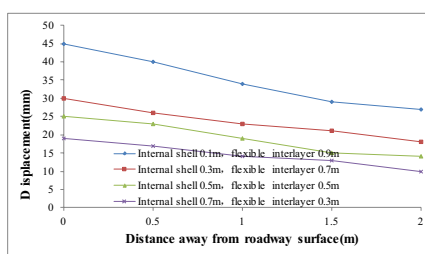
(a) Internal shell 0.1m, flexible interlayer 0.9m

(b) Internal shell 0.3m, flexible interlayer 0.7m

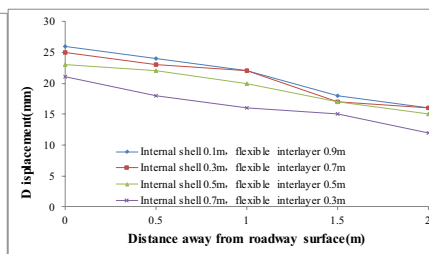


(c) Internal shell 0.5m, flexible interlayer 0.5m

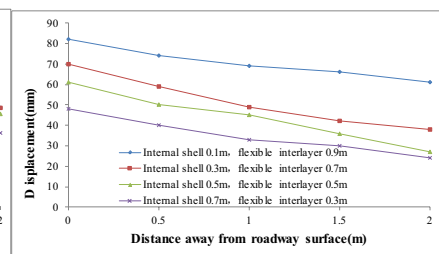
(d) Internal shell 0.7m, flexible interlayer 0.3m



(e) Roof lowering



(f) Floor heave



(g) Relative displacement between two sides

Fig. 15 Displacement distribution of different location away from the roadway’s surface

refer to displacements of roof rocks at different depths. Each displacement was the average of the values from the three observation stations point represents.

The crossing observation method was used to get the surface displacement of roadway. The changed values of displacement between OB were the floor heaves; the changed

values of displacement between CD were the relative displacement of two sides and the changed values of displacement between OA were the roof lowering. The principle of crossing observation method is shown in Fig. 18a. Roof separation behavior in the roadway was monitored using the multi-point roof extensometer displayed in Fig. 18b, which

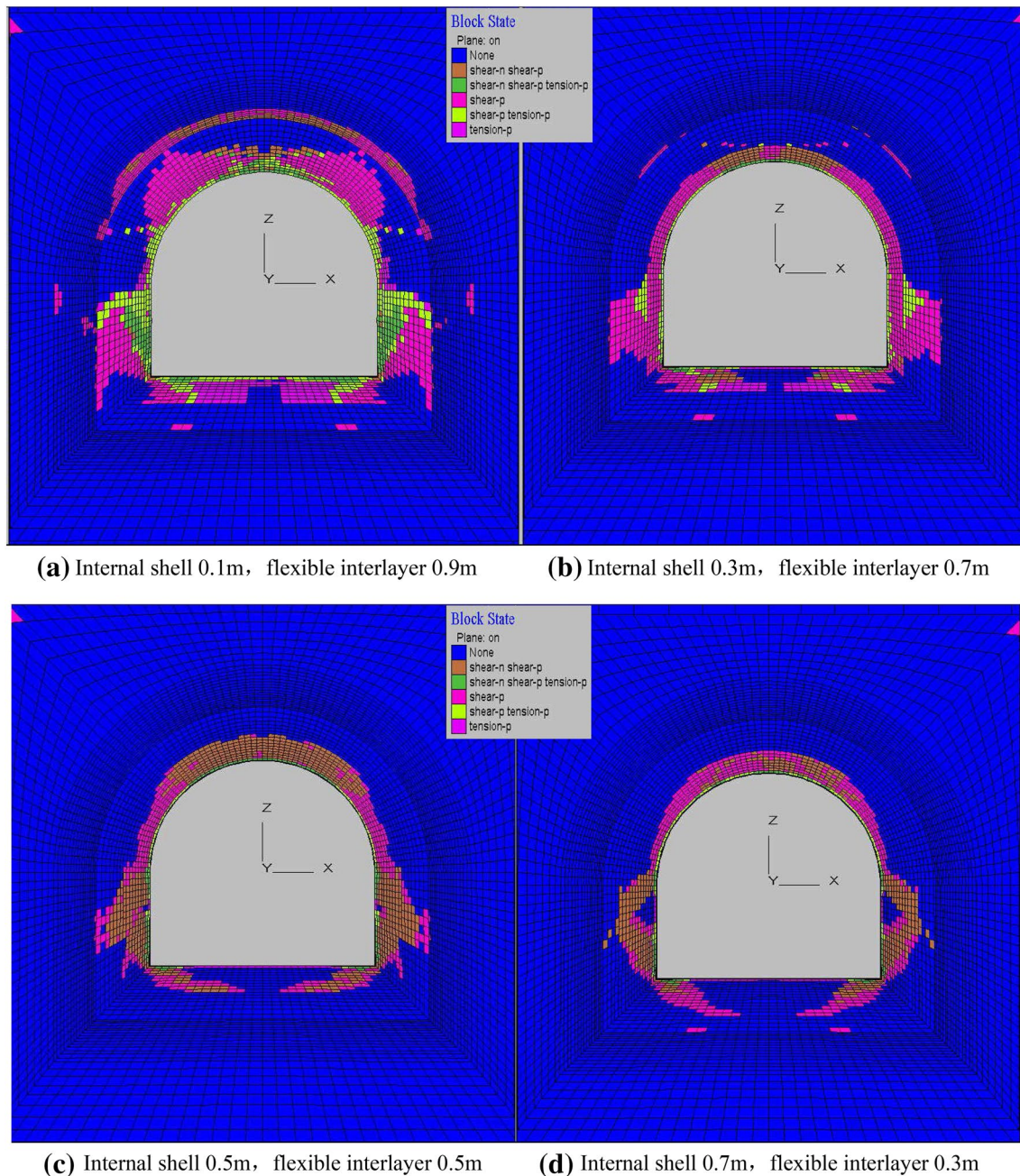


Fig. 16 The distribution of plastic zones

can measure the roof separations in four layers located 1.5, 3, 4.5, and 6 m from the surface of the abandoned roadways, respectively.

Figure 19 demonstrates that the floor heave leveled off 16–18 days after completion of the support construction and ultimately reached a maximum of 82 mm. The relative displacement between two sides and roof lowering became stable 50–52 days after completion of the support

construction and peaked at 185 and 161 mm, respectively. The displacement of interior roof strata decreased with increasing distance from the roof surface. It took less time to stabilize roof strata at longer distances. The maximum displacements measured at different locations did not exceed 5% of corresponding dimensions of the roadway's cross section, indicating that the support method

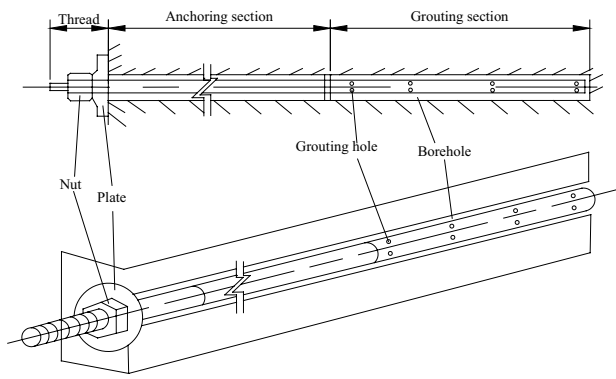


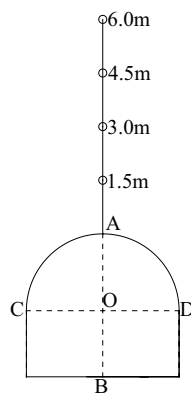
Fig. 17 Grouting bolt schematic diagram

proposed has effectively stabilized the surrounding rocks and can be used to achieve roadway stability.

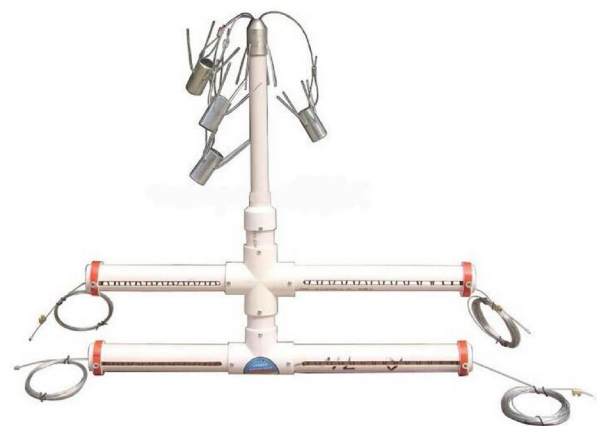
Conclusions

1. A mechanical model of vertical-wall, semicircular-arched roadway was created to illustrate the stresses in the rocks surrounding the roadway. Formulas describing stresses in the surrounding rocks were derived through complex analysis. The stress distribution in the surrounding rocks predicted by the formulas shows that stress concentration zones are distributed at the two lower corners of the roadway and the two spandrels over the arch. The four zones should be given special attention in surrounding rock control.
2. The North 1 main roadway of the Duerping coal mine has suffered severe damage and the conventional support method employed there is incapable of ensuring long-term stability of the surrounding rocks. A double-shell support structure was developed as a new technique for surrounding rock control. The functional mechanisms of the internal shell, flexible interlayer, and external shell

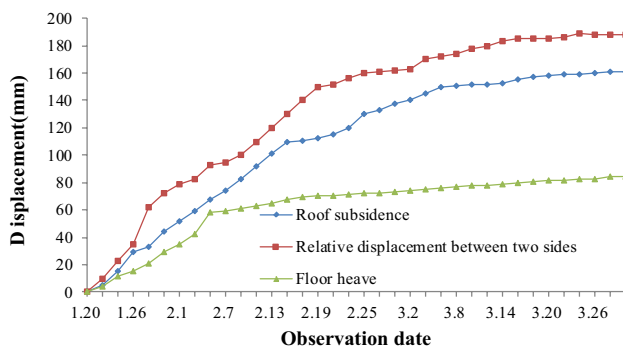
Fig. 18 The method and meter of deformation in roadway



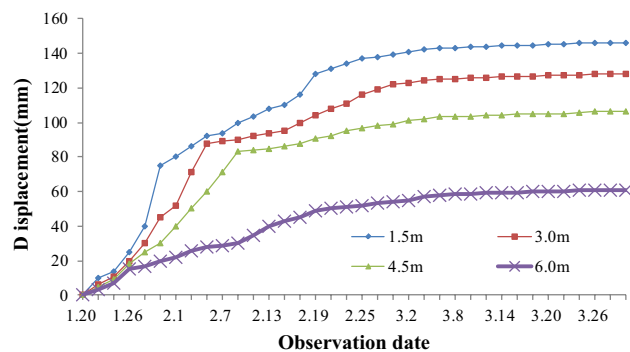
(a) Crossing observation method



(b) Multi-point roof extensometer



(a) Surface displacement



(b) Deep base point displacement

Fig. 19 Variations in measured roadway deformation

of this structure and the specific construction procedure were analyzed.

3. The stress–deformation–failure characteristics of the surrounding rocks for different shell and interlayer thicknesses were numerically analyzed using FLAC3D. A comparative analysis of the numerical results suggests that the optimal thicknesses for the external shell, internal shell, and flexible interlayer are 0.8, 0.3, and 0.7 m, respectively.
4. The double-shell support technique was experimentally implemented along a section of the North 1 main roadway. The grout and shotcrete for the internal and external shells were prepared from cement and sodium silicate. The shotcrete was sprayed with a type of blast-proof shotcrete machine for wet spraying. The grout was placed using grouting bolts and hydraulic grouting pumps. The measurements of surface and deep base point displacements show that after implementation of this technique, the floor heave, relative displacement between two sides, and roof lowering in this roadway decreased to 82, 185, and 161 mm, respectively, which can ensure long-term stability of the roadway. This verifies the effectiveness of the proposed technique in surrounding rock control.

Acknowledgements Financial support for the Fundamental Research Funds for the Central Universities (No. 2015QNB11), the Priority Academic Program Development of Jiangsu Higher Education Institutions (PAPD). The authors gratefully acknowledge financial support of the above items.

References

- Bjorkman GS, Richards R (1976) Harmonic holes—an inverse problem in elasticity. *J Appl Mech* 43(3):414–418
- Bjorkman GS, Richards R (1979) Harmonic holes for nonconstant fields. *J Appl Mech* 46(3):573–576
- Bloor AS (2013) Deformation of a circular concrete roadway lining in response to strata movement. *Strata Mech* 32:223
- Chen ZY (1994) Mechanical analysis of surrounding rock. Coal Industry Publishing House, Beijing
- Cristescu ND, Paraschiv I (1995) The optimal shape of rectangular-like caverns. *Int J Rock Mech Min Sci Geomech Abstr* 32(4):285–300
- Feng W, Han LJ, Liu CC (2012) Influence of horizontal stress on stress distribution and deformation characteristics around arched roadway. *J Saf Sci Technol* 8(12):21–26
- Goursat E (1898) Leçons sur l'intégration des équations aux dérivées partielles du second ordre à deux variables indépendantes. A. Hermann
- Guo WY, Zhao TB, Tan YL et al (2017) Progressive mitigation method of rock bursts under complicated geological conditions. *Int J Rock Mech Min Sci* 96:11–22
- He ZL, Qu B (2016) Simulation analysis of floor stress under different lateral pressure coefficients in vertical-wall, semicircular-arch (VWSA) roadway. *Min Technol* 16(4):38–39 (in Chinese)
- Kim BH, Larson MK, Lawson HE (2018) Applying robust design to study the effects of stratigraphic characteristics on brittle failure and bump potential in a coal mine. *Int J Min Sci Technol*
- Koyama Y (2003) Present status and technology of shield tunneling method in Japan[J]. *Tunn Undergr Space Technol* 18(2):145–159
- Lv AZ, Zhang LQ (2007) Underground tunnel mechanics analysis of complex function method. Science Press, Beijing
- Muskhelishvili NI (2013) Some basic problems of the mathematical theory of elasticity. Springer, Berlin
- Pengfei J, Jian L, Bin H et al (2016) The deformation mechanism and support methods of the water-bearing soft rock roadway. *Phys Numer Simul Geotech Eng* 22:55
- Richards R, Bjorkman GS (1980) Harmonic shape and optimum design. *J Eng Mech Div* 106(6):1125–1134
- Sears MM, Rusnak J, Van Dyke M et al (2017) Coal rib response during bench mining: a case study. *Int J Min Sci Technol*
- Shan RL, Kong XS, Bin LI, Shan P, Xia Y (2014) Supporting design and optimization of large section roadway with straight wall and semicircle arch. *China Min Mag* 23(1):87–91
- Shuancheng GU, Enbo W, Xiangdong SHI (2014) Spandrel failure mechanism analysis of arched roadway in layered rock mass. *Saf Coal Min* 11:050
- Zang CW, Ma CL, Zhuang XA (2012) Research and application of full-length grouted anchor in roadway under mining face. *Adv Mater Res Trans Tech Publ* 468:2872–2877